Biosensors and Bioelectronics 142 (2019) 111529

Contents lists available at ScienceDirect

Biosensors and Bioelectronics

journal homepage: www.elsevier.com/locate/bios

Sensitive electrochemical sensor for nitrite ions based on rose-like AuNPs/MoS_2/graphene composite

Yujie Han, Ran Zhang, Chuan Dong, Fangqin Cheng, Yujing Guo*

Institute of Environmental Science, Shanxi University, Taiyuan, 030006, China

ARTICLE INFO

Keywords:
MoS_2
Graphene
AuNPs
Electrochemical sensor
Nitrite detection

ABSTRACT

Nitrite ions (NO_2^-) have been widely used in the food and drink industry as preservatives. However, the NO_2^- discharged into the environment is harmful to the ecosystem and human health. Due to its potential toxicity, selective and sensitive detection of nitrite is important. In this work, a rose-like Au nanoparticles/MoS_2 nanoflower/graphene (AuNPs/MoS_2/GN) composite was fabricated using a one-pot hydrothermal method without the addition of any extra reductant for use in nitrite detection. Graphene acts as an efficient matrix for the growth of MoS_2 nanoflower (NF), and the edges of the MoS_2 NF subsequently load AuNPs. The obtained AuNPs/MoS_2/GN composite exhibits excellent electrooxidative activity toward nitrite ions, which is attributable to its large specific surface area, good conductivity, and the synergistic catalysis of each component. Accordingly, we propose a rapid, sensitive, and cost-effective electrochemical method for nitrite detection, which achieved a linear dynamic range of 5.0 μM to 5.0 mM with a detection limit of 1.0 μM. The present work provides not only a general one-pot synthesis method for a variety of noble–transition metal dichalcogenides nanohybrids, but also an example of the fabrication of an electrochemical nitrite sensor using a nanohybrid as an enhanced material, an approach that can easily be extended to other sensors.

1. Introduction

The overuse of sodium nitrite as a preservative in the food and drink industry accompanied by excessive discharge causes harm to the ecosystem and human health (Plumere, 2013). According to the World Health Organization (WHO), the fatal level of nitrite ions (NO_2^-) is 8.7–28.3 μM (Sudarvizhi et al., 2018). Thus, a selective and sensitive nitrite detection method is urgently needed (Manoj et al., 2018). So far, several analytical techniques have been developed for NO_2^- detection, such as chromatography mass spectrometry (Pagliano et al., 2012), spectrophotometry (Zhang et al., 2018a), chromatography (Liu et al., 1996), chemiluminescence (Dong et al., 2013; Nevin Öztekin 2002), and electrochemistry (Ghanei-Motlagh and Taher, 2018; Stanković et al., 2016). Among these approaches, the electrochemical technique has received extensive attention due to advantages such as rapid response, low cost, reliable and sensitive analysis, and facile operation modes. The different reduction products of NO_2^- rely on the condition of the electrodes, the components, and the morphology of the catalysts. There are two ways to measure NO_2^-: anodic oxidation of NO_2^- to NO_3^- and cathodic reduction of NO_2^-. In the anodic oxidation reaction, NO_3^- is generated without interference from other elements or anions, while the cathodic reduction of NO_2^- suffers from co-existence of the reduction peaks of dissolved products such as O_2 and NO. Hence, anodic oxidation is preferable.

Graphene (GN) has attracted considerable attention due to its large surface area, high electrical conductivity, good chemical stability, and mechanical strength (Kuila et al., 2012; Whitby, 2014). These distinctive features make GN-based materials promising for use in electrodes, which have been widely employed in electrocatalysis (Pumera et al., 2010). Nevertheless, irreversible agglomeration readily occurs in pure GN due to the π–π stacking interactions and van der Waals energy (Deepthi Konatham, 2008). Thus, chemical modification of GN with nanoparticles (NPs) or their alloys was proposed to overcome this drawback (Jiang et al., 2014; Jian et al., 2018; Li et al., 2012).

Ever since the discovery of GN, various two-dimensional materials have been studied extensively (Dong et al., 2018; Sinha et al., 2018). In recent years, MoS_2 have drawn considerable attention due to their ultrathin structure (Bertolazzi et al., 2018; Geng and Yang, 2018). In MoS_2 nanosheets, hexagonal Mo-atom layers are arranged between S-atom layers, and excellent crystal, optical, and catalytic properties are obtained (Joswig et al., 2015). Compared with the electronic active sites in GN, those in MoS_2 are usually distributed on the edges, and the conductivity is relatively low (Mani et al., 2016; Wang et al., 2015; Xu et al., 2013). Thus, the morphology and/or electronic structure of MoS_2

* Corresponding author.
E-mail address: guoyj@sxu.edu.cn (Y. Guo).

https://doi.org/10.1016/j.bios.2019.111529
Received 12 July 2019; Accepted 20 July 2019
Available online 22 July 2019

nanosheets are often adjusted to improve their electrochemical performance. Surfactants or carbon-based materials can induce the controllable formation of MoS_2 nanoflower (NF) (Huang et al. 2017a, 2017b; Zhang et al. 2018b, 2018c), which enlarges the surface area and promotes greater exposure of active sites. The electronic structure can be adjusted by tuning the crystal phase, introducing heteroatoms, vacancies, or defect sites, which may regulate the electrochemical properties of MoS_2 nanosheets (Huang et al., 2018; Miralrio et al., 2018; Sun and Wang, 2018; Xue et al., 2017). These strategies have led to the successful preparation of numerous MoS_2 with improved electrochemical performance. Recently, composites with MoS_2 grown on GN, carbon nanotubes, or carbon fibers have been synthesized and have exhibited enhanced electrochemical behavior, higher electron conductivities, and larger surface areas (Bian et al., 2012; Wang et al., 2016; Zhang et al., 2012) than either separate component. In addition, due to their superior electrical and catalytic characteristics, AuNPs have received considerable attention in many applications, such as sensors (Xu et al., 2015) and catalysis (Han et al., 2012). Inspired by the properties of each component, the combination of AuNPs with MoS_2 or GN may lead to the development of flexible nano-assembled systems with enhanced electrochemical performance. Some research has already been reported on AuNPs/MoS_2 and AuNPs/GN composite-based electrochemical sensor devices (Devi et al., 2019; Huang et al., 2016; Li et al., 2019; Wang et al., 2013; Wang et al., 2018). However, only a few studies have focused on AuNPs/MoS_2/GN for electrochemical sensors (Sharifuzzaman et al., 2019; Zhao et al., 2019), and most of them have involved the use of an additional reductant to reduce AuNPs onto the MoS_2/GN surface.

In this study, we developed a simple and efficient nitrite sensor based on a rose-like AuNPs/MoS_2/GN modified glassy carbon electrode (AuNPs/MoS_2/GN/GCE) synthesized via a one-pot method without any additional reductant. The MoS_2 NF with AuNPs grown on the edges was anchored onto the surface of GN successfully via a hydrothermal method. AuNPs/MoS_2/GN/GCE showed good electrocatalytic activity for nitrite oxidation and thus could be used as an effective nitrite sensor, which could also be employed for detection in actual samples.

2. Materials and methods

2.1. Materials

Ammonium molybdate ($(NH_4)_6Mo_7O_{24}{\cdot}4H_2O$), thiourea ($CS(NH_2)_2$), polyvinyl pyrrolidone (PVP, K30), ammonia solution, hydrazine (80% w/w), $HAuCl_4$, $NaNO_2$, Na_2HPO_4, NaH_2PO_4, KNO_3, Na_2SO_4, $CaCl_2$, $NaClO_4$, KCl, and glucose were purchased from Aladdin Chemical Reagent Company (Shanghai, China). All of the chemical reagents were analytical grade and were used without further purification. Ultrapure water was used throughout the experiment.

2.2. Instruments

Transmission electron microscopy (TEM) was conducted using a TECNAI G2 F20 TEM with an accelerating voltage of 200 kV. X-ray photoelectron spectroscopy (XPS) measurements were performed using an ESCALAB-MKI I spectrometer (VG Co., United Kingdom) with Al Kα X-ray radiation as the X-ray source for excitation. The Brunauer–Emmett–Teller (BET) surface areas and nitrogen sorption isotherms were measured using an ASAP 2020 Physisorption Analyzer (Micromeritics Instrument Corporation, USA). Raman measurements were conducted using a LabRAM HR Evolution spectrometer (Renishaw inVia plus, United Kingdom) with 514 nm laser excitation. XRD patterns were recorded on a D8 ADVANCE (BRUKER, Germany) diffractometer using Cu Ka radiation with a Ni filter (λ = 0.154059 nm at 40 kV and 40 mA).

All of the electrocatalytic measurements were performed on a CHI660C electrochemical workstation (Chenhua Instruments Corp., Shanghai, China) at room temperature. A conventional three-electrode configuration was used, including a modified GCE (with a diameter of 3.0 mm) as the working electrode, a saturated calomel electrode (SCE) as the reference electrode, and a Pt wire counter electrode.

2.3. GN preparation

GN was synthesized according to the literature (Guo et al., 2012). In short, 75 mg of PVP powder was added to 22 mL of homogeneous graphite oxide (GO) solution (0.25 mg mL^{-1}, Li et al., 2008) under stirring for 1 h. Then, 200 μL of concentrated ammonia solution and 20 μL of hydrazine solution (80% w/w) were added to the above solution, which was stirred for an additional 40 min. The mixture underwent a water bath for 1 h at 90 °C, and GO was reduced to GN. The final GN solution was centrifugated and washed with ultrapure water twice each and dispersed in water again for further use.

2.4. One-pot synthesis of rose-like AuNPs/MoS_2/GN composite

The rose-like AuNPs/MoS_2/GN composite was synthesized as described in the literature, with slight modification (Chen et al., 2017a). The mixture of $(NH_4)_6Mo_7O_{24}{\cdot}4H_2O$ (1.0 mmol), $CS(NH_2)_2$ (30 mmol), and $HAuCl_4$ (1.0 mmol) was dispersed in 17.5 mL of PVP-GN solution (1.0 mg mL^{-1}) and stirred vigorously at room temperature for 1 h. The mixture was then transferred into a 50 mL Teflon-lined stainless-steel autoclave and heated at 180 °C for 24 h to obtain the rose-like AuNPs/MoS_2/GN composite. After cooling down to room temperature, the composites were collected by centrifugation and washed with ultrapure water and ethanol several times successively, then dried at 70 °C under a vacuum. For comparison, MoS_2 NF/GN composite was synthesized under the same conditions without adding Au precursor.

2.5. Preparation of AuNPs/MoS_2/GN/GCE and electrochemical measurements

Before modification, the GCE was polished with 1, 0.3, and 0.05 μm alumina slurry on a polishing cloth. It was thoroughly rinsed with an alcohol/water (1:1) mixture followed by sonication before use. The as-prepared AuNPs/MoS_2/GN, MoS_2 NF/GN, and GN composites were dispersed in water under ultrasonication to form homogeneous solutions (1.0 mg mL^{-1}). A certain amount of AuNPs/MoS_2/GN composite was cast onto the pretreated GCE surface. For comparison, the MoS_2 NF/GN- or GN-modified GCE (MoS_2 NF/GN/GCE, GN/GCE) was prepared using the same procedure with the same modification of the composite quantities. Scheme 1 illustrates the synthesis of AuNPs/MoS_2/GN as well as the sensing of $NaNO_2$.

The electrochemical measurements were performed by cyclic voltammetry (CV) and amperometry in a phosphatic buffer (0.1 M PBS, pH 4.0) containing $NaNO_2$.

3. Results and discussion

3.1. Characterization of as-prepared AuNPs/MoS_2/GN

The morphology and microstructure of the as-prepared composites were characterized via TEM. As shown in Fig. 1A and B, the rose-like MoS_2 flakes were anchored onto the GN surface uniformly. Here, the GN sheets acted as a pliable substrate for the uniform growth of MoS_2 NF. The MoS_2 NF formed due to the hydrothermal reaction condition and the $(NH_4)_6Mo_7O_{24}{\cdot}4H_2O$ precursors used in the reaction. During the hydrothermal procedure, $(NH_4)_6Mo_7O_{24}{\cdot}4H_2O$ released MoO_4^-, which has a layered structure. When MoO_4^- ions react with sulfide ions, the intercalation of residual ammonia between the different layers helps prevent the stacking of MoS_2 sheets, which leads to the formation of a sphere-like shape (Krishnamoorthy et al., 2014). The MoS_2 NFs, with an average diameter of 100 nm, consisted of numerous folded

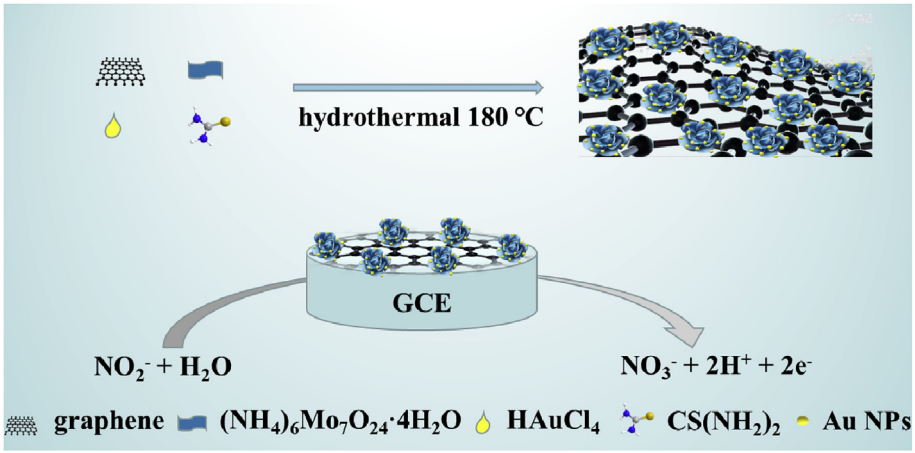

Scheme 1. Schematic illustration of one-pot synthesis of the AuNPs/MoS_2/GN composite and the electrochemical sensing procedure for nitrate.

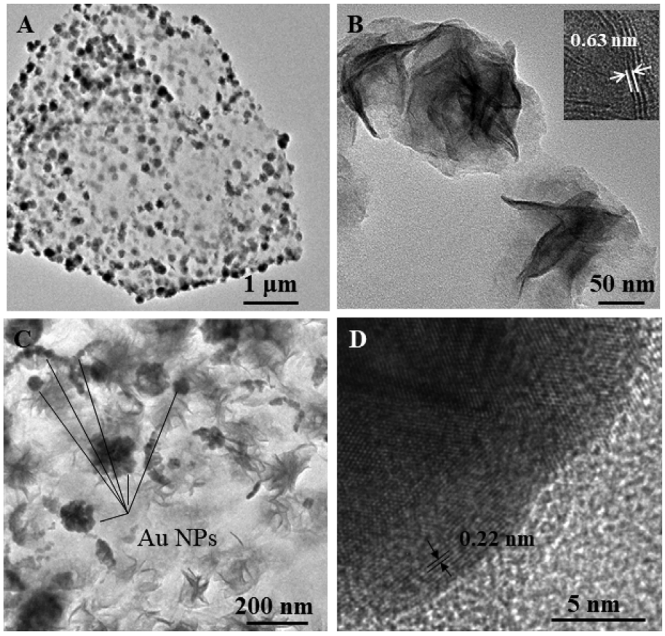

Fig. 1. TEM images of as-prepared MoS_2 NF/GN (A and B, the inset is the HRTEM image of MoS_2 sheets) and AuNPs/MoS_2/GN (C) and HRTEM image of AuNPs in AuNPs/MoS_2/GN (D).

edges, maximizing the exposure of active sites. The inset in Fig. 1B is a high-resolution TEM (HRTEM) image of the MoS_2 sheets, which shows the parallel layers of MoS_2 sheets perpendicular to the [002] direction, and the interlayer distance is 0.63 nm. The morphology of the obtained AuNPs/MoS_2/GN is shown in Fig. 1C. AuNPs obviously formed around the edges of the MoS_2 NF with a uniform size of about 20 nm, which may be due to the high density of energetic defects at the edges of the MoS_2 nanosheets (Xu et al., 2013). The clear interplanar spacing of 0.22 nm corresponds to the (111) planes of Au.

The chemical compositions of the as-synthesized AuNPs/MoS_2/GN, MoS_2 NF/GN, and GN were further determined by XPS and X-ray powder diffraction (XRD). As shown in the XPS survey spectrum, AuNPs/MoS_2/GN contained Mo, S, C, N, O, and Au (Fig. 2A). Specifically, the deconvoluted C1s spectrum (Fig. 2B) shows three peaks at 284.7 eV (C═C), 286.7 eV (C–N/C–O), and 288.9 eV (C═O) (Guo et al., 2012). The amount of C–O groups is relatively low, indicating that GO is reduced during the hydrothermal procedure. Three O-related species—C═O (531.2 eV), C–O or C–O–Mo (532.2 eV), and hydroxyl groups (533.5 eV)—are observable in the deconvoluted O 1s XPS spectrum (Fig. 2C). The binding energies located at 229.6 eV and 232.6 eV represent Mo $3d_{5/2}$ and Mo $3d_{3/2}$, respectively, corresponding to the Mo^{4+} in MoS_2 and a small amount of Mo^{5+} (Fig. 2D) (Xiong et al., 2015). Peaks at 162.5 eV and 163.6 eV, which are related to S $2p_{3/2}$ and S $2p_{1/2}$ of divalent sulfide ions, are clearly observable in Fig. 2E (Qiao et al., 2016). Fig. 2F shows the XPS signature of the Au 4f doublet ($4f_{7/2}$ and $4f_{5/2}$) for the AuNPs supported on GN sheets (Li et al., 2015). Additionally, the XPS spectrum of AuNPs/MoS_2/GN was compared to those of MoS_2 NF/GN and GN. As shown in Fig. S1, the XPS binding energies of O 2p, N 1s, and C 1s in AuNPs/MoS_2/GN, MoS_2 NF/GN, and GN exhibit negligible shifts, suggesting there is negligible covalent bonding among the AuNPs, MoS_2 NFs, and GN. The binding energies of Mo 3d in AuNPs/MoS_2/GN and MoS_2 NF/GN are consistent as well, demonstrating that there is no obvious interaction between the Mo and Au atoms. The peak intensity of S 2p slightly differs between AuNPs/MoS_2/GN and MoS_2 NF/GN because of the formation of Au–S covalent bonds. In the XPS spectrum of AuNPs/MoS_2/GN, a characteristic peak of Au is visible, confirming the successful anchoring of the AuNPs in AuNPs/MoS_2/GN.

To understand the effects of MoS_2 NF and AuNPs on GN organization, we performed Raman spectroscopic analysis to characterize the structures of GN, MoS_2 NF/GN, and AuNPs/MoS_2/GN (Fig. S2). The D band is generated by the vibration of C atoms with dangling bonds in the plane terminations of disordered graphite, and the G band arises from the in-plane stretching of ordered sp^2-bonded C atoms in the C hexagonal lattice (Jian et al., 2018). The ratio between the intensity of the D band and that of the G band (I_D/I_G) indicates the defect level in C materials. I_D/I_G was obtained from the Raman analysis of GN (I_D/I_G = 1.08), MoS_2 NF/GN (I_D/I_G = 1.04), and AuNPs/MoS_2/GN (I_D/I_G = 1.02). The Raman shifts in the D band, G band, 2D band, and D + D′ band of GN are consistent with MoS_2 NF/GN and AuNPs/MoS_2/GN. Basically, AuNPs could enhance the Raman intensity (Biroju and Giri, 2014). However, only a small amount of Au precursor was added, inducing slight enhancement of the Raman intensity. Consequently, the Raman analysis demonstrates that the incorporation of MoS_2 NFs and AuNPs has little influence on the GN organization.

The XRD pattern of AuNPs/MoS_2/GN is displayed in Fig. S3. The peaks at 44.39, 64.54, and 77.65 correspond to the (200), (220), and (311) planes of AuNPs (JCPDS 4–0783) and the peaks at 32.32, 38.16, 52.31, and 57.59 can be assigned to the (101), (104), (018), and (110) planes of MoS_2 (JCPDS 74–0932). In the XRD spectrum of GN, a slight peak appears at $2\theta = 24.3^\circ$, demonstrating that GO was reduced to GN (Li et al., 2012).

Due to the 3D architecture, AuNPs/MoS_2/GN has a large surface area and more exposed S–Mo–S electroactive edges. The surface areas of the as-synthesized AuNPs/MoS_2/GN and commercial MoS_2 were confirmed by BET analysis (Fig. S4). The obtained curve agreed with a

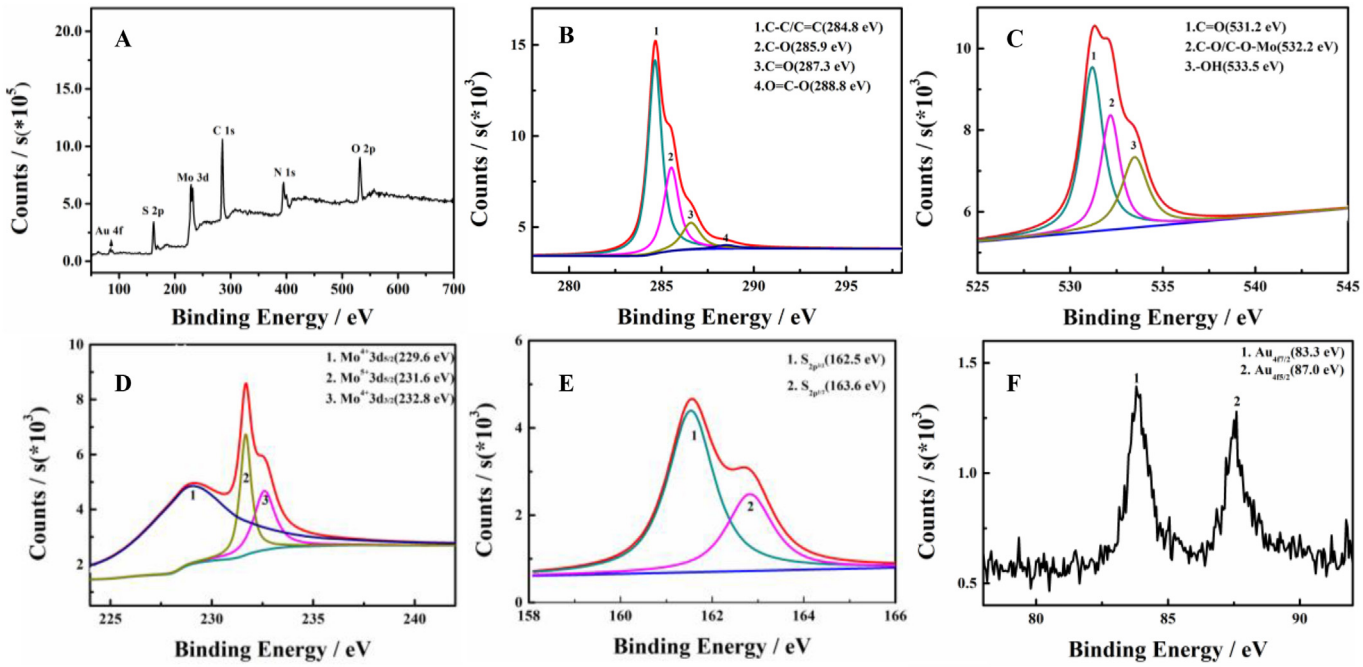

Fig. 2. Full XPS spectrum (A) and deconvoluted C 1s (B), O 1s (C), Mo 3d (D), S 2p (E), and Au 4f (F) XPS spectra of as-prepared AuNPs/MoS_2/GN.

typical type-IV isotherm with a hysteresis loop (IUPAC classification) (Chen et al., 2017b) from a relative pressure of 0.44–0.98, suggesting that AuNPs/MoS_2/GN has microspores and a mesoporous structure. Due to the stacked layers, the BET surface area of AuNP/MoS_2/GN was found to be about 43.84 $m^2 g^{-1}$, which is about two times higher than that of commercial MoS_2 (19.45 $m^2 g^{-1}$). This enlarged surface area combined with more exposed electroactive S–Mo–S edges may contribute to the enhanced catalytic activity with $NaNO_2$. The corresponding average pore width was distributed from 30 nm to 40 nm, indicating that such a microporous structure is conductive to electrocatalytic activity because it is beneficial for electron and ion diffusion.

3.2. Electrocatalytic behavior of AuNPs/MoS_2/GN towards $NaNO_2$

The electrochemical behaviors of an AuNPs/MoS_2/GN-modified GCE were investigated via CV in 0.1 M PBS (pH 4.0) in the presence of 1.0 mM $NaNO_2$ (Fig. 3A). A large oxidation peak of 0.75 V (vs. SCE) appears in the presence of $NaNO_2$ (black solid line). For comparison, the electrooxidation of a MoS_2 NF/GN/GCE, GN/GCE, and bare GCE towards $NaNO_2$ was also investigated. The oxidation peaks of $NaNO_2$ for the MoS_2 NF/GN/GCE, GN/GCE, and bare GCE are located at 0.79, 0.78, and 0.88 V, respectively, which are more positive than that of the AuNPs/MoS_2/GN/GCE. Therefore, AuNPs/MoS_2/GN exhibited superior electrooxidation activity toward $NaNO_2$ and thus made it possible to develop an electrochemical nitrite sensor.

To promote the sensitivity of the constructed electrochemical $NaNO_2$ sensor, we optimized the experimental conditions. Firstly, the effects of pH and the amount of AuNPs/MoS_2/GN on $NaNO_2$ were investigated (Figs. S5A and B), indicating that the nitrite oxidation current was affected by the pH. This dependence was further studied using CV in 0.1 M PBS solution containing 1.0 mM nitrite at different pH values (pH 3.0–7.0). As shown in Fig. S5A, the oxidation current increased with increasing pH up to 4.0 and decreased from pH 4.0 to pH 7.0. Thus, pH 4.0 was chosen in the following measurements. The oxidation current at pH values less than 4.0 may be due to the conversion of NO_2^- to NO and NO_3^- (Wang and Hui, 2017) or the protonation of NO_2^- (Afkhami et al., 2012). A decrease in the peak current at pH values greater than 4.0 is due to the decrease in the reduction of

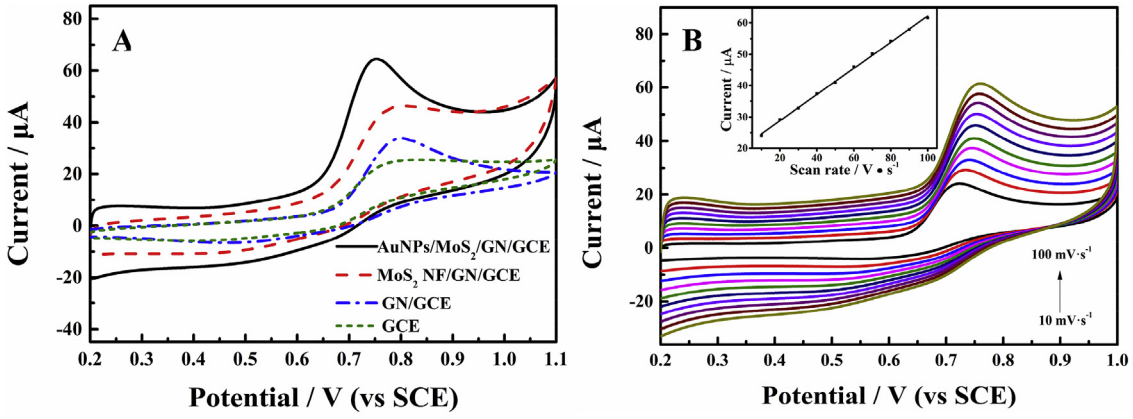

Fig. 3. (A) CV results for bare GCE (—), GN/GCE (— -), MoS_2 NF/GN/GCE (— —), and AuNPs/MoS_2/GN/GCE (–) in 0.1 M PBS containing 1.0 mM $NaNO_2$ with a scan rate of 50 mV s^{-1}. (B) CV results for AuNPs/MoS_2/GN/GCE in 0.1 M PBS (pH 4.0) in the presence of 1.0 mM $NaNO_2$ with different scan rates. The inset shows the peak current vs. scan rate.

nitrate to nitrite, which reduces the NO_2^- concentration at the AuNPs/MoS_2/GN surface (Salimi et al., 2014). The peak potential is not affected much by the pH of the solution, which is consistent with a previous report (Ghanei-Motlagh and Taher, 2018). The reason for this difference could be the fact that the oxidation mechanism is a kinetically controlled process (Peng et al., 2017). After optimizing the pH, we checked the effects of different quantities of AuNPs/MoS_2/GN on the oxidation current. The results show that the modified GCE with 6.0 μL of AuNPs/MoS_2/GN had better catalytic properties than those with other amounts. Thus, we choose pH 4.0 and a modified GCE with 6.0 μL AuNPs/MoS_2/GN for the following electrochemical detection.

CV measurements of electrocatalysis toward $NaNO_2$ oxidation at different scan rates were also performed. Fig. 3B demonstrates that the anodic current of $NaNO_2$ is proportional to the scan rate in the range of 0.01–0.1 V s^{-1} in 0.1 M PBS (pH 4.0), indicating the dominance of the surface-controlled process, which is in agreement with previous findings (Lu, 2019; Wang et al., 2014).

The number of electrons involved in this reaction was calculated based on the linear relationship between the oxidation peak potential (E_p) and the logarithm of the scan rate (logν) (see Fig. S6) (Lu, 2019):

$$E_p = \frac{2.303RT}{2(1-a)nf}\log v + K$$

where n is the number of electrons participating in the reaction; υ is the scan rate (mV·s^{-1}); α is the electron transfer coefficient, which was calculated using a Tafel plot (Sudarvizhi et al., 2018), yielding a value of 0.36 for AuNPs/MoS_2/GN/GCE; finally, f, R, and T are Faraday's constant (96,500 C mol^{-1}), the universal gas constant (8.314 J mol^{-1} K^{-1}), and the temperature (298 K), respectively. The linear fitting equation is $E_p = 0.042\log\nu + 0.68$. n was calculated to be 2.1 ≈ 2, indicating a two-electron transfer process during NO_2^- oxidation.

3.3. Electrochemical detection of $NaNO_2$ at AuNPs/MoS_2/GN modified electrode

Due to the attractive electrooxidation activity of AuNPs/MoS_2/GN towards $NaNO_2$, a biosensor for $NaNO_2$ detection was developed. Electrochemical sensing of $NaNO_2$ was performed using amperometry of an AuNPs/MoS_2/GN-modified electrode at 0.75 V in 0.1 M PBS (pH 4.0). Fig. 4A shows a typical amperogram with the addition of different concentrations of $NaNO_2$. After the addition of $NaNO_2$, the AuNPs/MoS_2/GN/GCE responded rapidly and reached a steady state within 4 s. Moreover, the current increase towards $NaNO_2$ at the AuNPs/MoS_2/GN/GCE is proportional to the concentration of $NaNO_2$. A corresponding calibration curve was generated by plotting the oxidation peak current against the concentration of $NaNO_2$ (Fig. 4B), and the linear fitting equation for nitrite detection is Ip_c (μA) = 0.0029c (μM) + 3.65 (R^2 = 0.998). It is evident that the modified electrode has a wide linear response in a range from 5.0 μM to 5.0 mM with a detection limit of 1.0 μM (according to the experimental result, from a visual evaluation), which is lower than or comparable to those of other noble metal NP-based or C material-based $NaNO_2$ electrochemical sensors (Table S1).

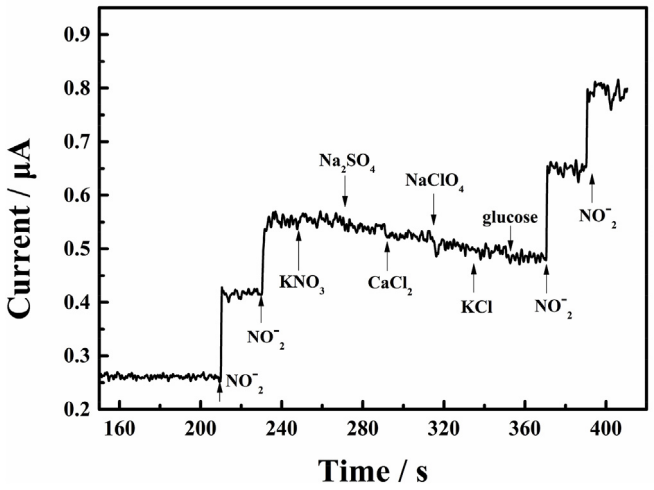

Fig. 5. Typical amperometric current responses at AuNPs/MoS_2/GN/GCE upon addition of 1.0 μM $NaNO_2$, 1.0 μM $NaNO_2$, 100.0 μM KNO_3, 100.0 μM Na_2SO_4, 100.0 μM $CaCl_2$, 100.0 μM $NaClO_4$, 100.0 μM KCl, 100.0 μM glucose, 1.0 μM $NaNO_2$, and 1.0 μM $NaNO_2$. Applied potential: 0.75 V.

To test the selectivity of the AuNPs/MoS_2/GN-modified electrode, some potential interfering substances that usually coexist with $NaNO_2$ in samples, such as KNO_3, Na_2SO_4, $CaCl_2$, $NaClO_4$, KCl, and glucose, were investigated. As shown in Fig. 5, unlike the obvious current increase with $NaNO_2$ injection, the current changes caused by the addition of these interferents were negligible, indicating the highly selective sensing of $NaNO_2$ with the AuNPs/MoS_2/GN/GCE. For 1.0 mM $NaNO_2$, the relative standard deviation (n = 4) was calculated to be 4.8%, indicating good repeatability. The stability of the constructed sensor was tested after the AuNPs/MoS_2/GN/GCE had been stored at 4 °C for 15 days. The peak current for 1.0 mM $NaNO_2$ decreased by only 8.0%, indicating that the constructed sensor has good stability.

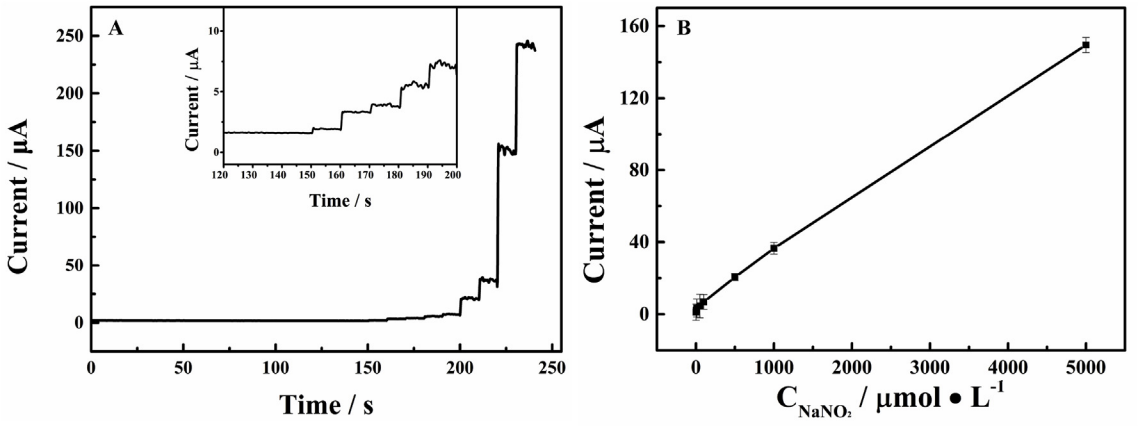

Fig. 4. (A) Amperometric current responses of AuNPs/MoS_2/GN/GCE upon successively stirring different amounts of $NaNO_2$ into 0.1 M PBS (pH 4.0). Applied potential: 0.75 V. (B) Linear calibration plot of the electrooxidation current of $NaNO_2$ vs. its concentration.

3.4. Actual sample detection

To investigate the practical applicability of the fabricated sensor, the concentrations of $NaNO_2$ in a sausage and pickle obtained from a local market were analyzed by using the standard addition method, and the results are presented in Table S2. The samples were prepared as described in previous literature (Yang et al., 2006), and the pretreated samples were diluted 100 times with 0.1 M PBS (pH 4.0). As shown in Table S2, the recovery values of the samples are between 98.0% and 103.2%. Therefore, the developed sensor could be applied for $NaNO_2$ concentration determination in actual samples.

4. Conclusions

In summary, a novel method of nitrite sensor fabrication based on a rose-like AuNPs/MoS_2/GN composite synthesized via an one-pot technique was demonstrated. The AuNPs/MoS_2/GN composite, which had a large surface area and high electrochemical conductivity and catalytic properties, exhibited enhanced electrochemical oxidation towards nitrite. The constructed sensor possessed a wide linear range from 5.0 μM to 5.0 mM, a low detection limit of 1.0 μM, high selectivity, good repeatability, and stability. However, the high overpotential still limits the practical use of the proposed sensor. In the future, we will investigate more MoS_2/GN-based composites and employ them in actual sample detection.

Declaration of competing interest

The authors declare that they have no known competing financial interests or personal relationships that could have appeared to influence the work reported in this paper.

CRediT authorship contribution statement

Yujie Han: Data curation, Formal analysis, Methodology, Writing - original draft. **Ran Zhang:** Data curation, Validation. **Chuan Dong:** Formal analysis. **Fangqin Cheng:** Validation. **Yujing Guo:** Formal analysis, Funding acquisition, Project administration, Supervision, Writing - review & editing.

Acknowledgement

This research work was supported by the National Natural Science Foundation of China (No. 21775095) and the Young “Sanjin” Scholar Foundation of Shanxi Province, 2016.

Appendix A. Supplementary data

Supplementary data to this article can be found online at https://doi.org/10.1016/j.bios.2019.111529.

References

Afkhami, A., Madrakian, T., Ghaedi, H., Khanmohammadi, H., 2012. Construction of a chemically modified electrode for the selective determination of nitrite and nitrate ions based on a new nanocomposite. Electrochim. Acta 66, 255–264.

Bertolazzi, S., Gobbi, M., Zhao, Y., Backes, C., Samori, P., 2018. Molecular chemistry approaches for tuning the properties of two-dimensional transition metal dichalcogenides. Chem. Soc. Rev. 47 (17), 6845–6888.

Bian, X., Zhu, J., Liao, L., Scanlon, M.D., Ge, P., Ji, C., Girault, H.H., Liu, B., 2012. Nanocomposite of MoS_2 on ordered mesoporous carbon nanospheres: a highly active catalyst for electrochemical hydrogen evolution. Electrochem. Commun. 22, 128–132.

Biroju, R.K., Giri, P.K., 2014. Defect enhanced efficient physical functionalization of graphene with gold nanoparticles probed by resonance Raman spectroscopy. J. Phys. Chem. C 118 (25), 13833–13843.

Chen, L., Yang, W., Liu, X., Jia, J., 2017a. Flower-like CoS_2/MoS_2 nanocomposite with enhanced electrocatalytic activity for hydrogen evolution reaction. Int. J. Hydrogen Energy 42 (17), 12246–12253.

Chen, M., Wu, P., Chen, L., Yang, S., Yu, L., Ding, Y., Zhu, N., Shi, Z., Liu, Z., 2017b. Three-dimensional multi-doped porous carbon/graphene derived from sewage sludge with template-assisted Fe-pillared montmorillonite for enhanced oxygen reduction reaction. Sci. Rep. 7 (1), 4158.

Deepthi Konatham, A.S., 2008. Molecular design of stable graphene nanosheets dispersions. Nano Lett. 8 (12), 4630–4641.

Devi, R., Gogoi, S., Barua, S., Sankar Dutta, H., Bordoloi, M., Khan, R., 2019. Electrochemical detection of monosodium glutamate in foodstuffs based on Au@MoS_2/chitosan modified glassy carbon electrode. Food Chem. 276, 350–357.

Dong, S., Guan, W., Lu, C., 2013. Quantum dots in organo-modified layered double hydroxide framework-improved peroxynitrous acid chemiluminescence for nitrite sensing. Sens. Actuators B Chem. 188, 597–602.

Dong, R., Zhang, T., Feng, X., 2018. Interface-Assisted synthesis of 2D materials: trend and challenges. Chem. Rev. 118 (13), 6189–6235.

Geng, D., Yang, H.Y., 2018. Recent advances in growth of novel 2D materials: beyond graphene and transition metal dichalcogenides. Adv. Mater. 30 (45), 1800865.

Ghanei-Motlagh, M., Taher, M.A., 2018. A novel electrochemical sensor based on silver/halloysite nanotube/molybdenum disulfide nanocomposite for efficient nitrite sensing. Biosens. Bioelectron. 109, 279–285.

Guo, Y., Han, Y., Shuang, S., Dong, C., 2012. Rational synthesis of graphene–metal coordination polymer composite nanosheet as enhanced materials for electrochemical biosensing. J. Mater. Chem. 22 (26), 13166–13173.

Han, J., Zhuo, Y., Chai, Y.Q., Yuan, Y.L., Yuan, R., 2012. Novel electrochemical catalysis as signal amplified strategy for label-free detection of neuron-specific enolase. Biosens. Bioelectron. 31 (1), 399–405.

Huang, H., Nie, R., Song, Y., Ji, Y., Guo, R., Liu, Z., 2016. Highly sensitive electrochemical sensor for tulobuterol detection based on facile graphene/Au nanowires modified glassy carbon electrode. Sens. Actuators B Chem. 230, 422–426.

Huang, M., Ouyang, L., Liu, J., Wang, H., Shao, H., Zhu, M., 2017a. Enhanced hydrogen generation by hydrolysis of Mg doped with flower-like MoS_2 for fuel cell applications. J. Power Sources 365, 273–281.

Huang, Q., Fang, Y., Shi, J., Liang, Y., Zhu, Y., Xu, G., 2017b. Flower-like molybdenum disulfide for polarity-triggered accumulation/release of small molecules. ACS Appl. Mater. Interfaces 9 (41), 36431–36437.

Huang, Y., Nielsen, R.J., Goddard, W.A., 2018. The reaction mechanism for the hydrogen evolution reaction on the basal plane sulfur vacancy site of MoS_2 using grand canonical potential kinetics. J. Am. Chem. Soc. 140 (48), 16773–16782.

Jian, J.M., Fu, L.F., Ji, J., Lin, L., Guo, X., Ren, T.L., 2018. Electrochemically reduced graphene oxide/gold nanoparticles composite modified screen-printed carbon electrode for effective electrocatalytic analysis of nitrite in foods. Sens. Actuators B Chem. 262, 125–136.

Jiang, J., Fan, W., Du, X., 2014. Nitrite electrochemical biosensing based on coupled graphene and gold nanoparticles. Biosens. Bioelectron. 51, 343–348.

Joswig, J.O., Lorenz, T., Wendumu, T.B., Gemming, S., Seifert, G., 2015. Optics, mechanics, and energetics of two-dimensional MoS_2 nanostructures from a theoretical perspective. Accounts Chem. Res. 48 (1), 48–55.

Krishnamoorthy, K., Veerasubramani, G.K., Radhakrishnan, S., Kim, S.J., 2014. Supercapacitive properties of hydrothermally synthesized sphere-like MoS_2 nanostructures. Mater. Res. Bull. 50, 499–502.

Kuila, T., Bose, S., Mishra, A.K., Khanra, P., Kim, N.H., Lee, J.H., 2012. Chemical functionalization of graphene and its applications. Prog. Mater. Sci. 57 (7), 1061–1105.

Li, D., Müller, M.B., Gilje, S., Kaner, R.B., Wallace, G.G., 2008. Processable aqueous dispersions of graphene nanosheets. Nat. Nanotechnol. 3 (2), 101–105.

Li, J., Liu, C.Y., Liu, Y., 2012. Au/Graphene hydrogel: synthesis, characterization and its use for catalytic reduction of 4-nitrophenol. J. Mater. Chem. 22 (17), 8426–8430.

Li, S.S., Hu, Y.Y., Wang, A.J., Weng, X., Chen, J.R., Feng, J.J., 2015. Simple synthesis of worm-like Au–Pd nanostructures supported on reduced graphene oxide for highly sensitive detection of nitrite. Sens. Actuators B Chem. 208, 468–474.

Li, X., Wu, D., Ma, H., Wang, H., Wang, Y., Fan, D., Du, B., Wei, Q., Zhang, N., 2019. Ultrasensitive amyloid-beta proteins detection based on curcumin conjugated ZnO nanoparticles quenching electrochemiluminescence behavior of luminol immobilized on Au@MoS_2/Bi_2S_3 nanorods. Biosens. Bioelectron. 131, 136–142.

Liu, Z.M., Xi, X.D., Dong, S.J., Wang, E.K., 1996. Liquid chromatography-amperometric detection of nitrite using a polypyrrole modified glassy carbon electrode doped with tungstodiphosphate anion. Anal. Chim. Acta 435, 153–157.

Lu, L., 2019. Highly sensitive detection of nitrite at a novel electrochemical sensor based on mutually stabilized Pt nanoclusters doped CoO nanohybrid. Sens. Actuators B Chem. 281, 182–190.

Mani, V., Govindasamy, M., Chen, S.M., Karthik, R., Huang, S.T., 2016. Determination of dopamine using a glassy carbon electrode modified with a graphene and carbon nanotube hybrid decorated with molybdenum disulfide flowers. Microchimica Acta 183 (7), 2267–2275.

Manoj, D., Saravanan, R., Santhanalakshmi, J., Agarwal, S., Gupta, V.K., Boukherroub, R., 2018. Towards green synthesis of monodisperse Cu nanoparticles: an efficient and high sensitive electrochemical nitrite sensor. Sens. Actuators B Chem. 266, 873–882.

Miralrio, A., Rangel Cortes, E., Castro, M., 2018. Electronic properties and enhanced reactivity of MoS_2 monolayers with substitutional gold atoms embedded into sulfur vacancies. Appl. Surf. Sci. 455, 758–770.

Oztekin, N., Nutku, M.S., Erim, F.B., 2002. Simultaneous determination of nitrite and nitrate in meat products and vegetables by capillary electrophoresis. Food Chem. 76 (1), 103–106.

Pagliano, E., Meija, J., Sturgeon, R.E., Mester, Z., D'Ulivo, A., 2012. Negative chemical ionization GC/MS determination of nitrite and nitrate in seawater using exact matching double spike isotope dilution and derivatization with triethyloxonium tetrafluoroborate. Anal. Chem. 84 (5), 2592–2596.

Peng, Z.W., Yuan, D., Jiang, Z.W., Li, Y.F., 2017. Novel metal-organic gels of bis

(benzimidazole)-based ligands with copper(II) for electrochemical selectively sensing of nitrite. Electrochim. Acta 238, 1–8.
Plumere, N., 2013. Interferences from oxygen reduction reactions in bioelectroanalytical measurements: the case study of nitrate and nitrite biosensors. Anal. Bioanal. Chem. 405 (11), 3731–3738.
Pumera, M., Ambrosi, A., Bonanni, A., Chng, E.L.K., Poh, H.L., 2010. Graphene for electrochemical sensing and biosensing. Trac. Trends Anal. Chem. 29 (9), 954–965.
Qiao, X., Hu, F., Hou, D., Li, D., 2016. PEG assisted hydrothermal synthesis of hierarchical MoS_2 microspheres with excellent adsorption behavior. Mater. Lett. 169, 241–245.
Salimi, A., Kurd, M., Teymourian, H., Hallaj, R., 2014. Highly sensitive electrocatalytic detection of nitrite based on SiC nanoparticles/amine terminated ionic liquid modified glassy carbon electrode integrated with flow injection analysis. Sens. Actuators B Chem. 205, 136–142.
Sharifuzzaman, M., Barman, S.C., Abu Zahed, M., San, N.J., Park, J.Y., 2019. Green synthesis of reduced graphene oxide decorated with few-layered MoS_2-nanoroses and Au/Pd/Ag trimetallic nanoparticles for ultrasensitive label-free ImmunosensingPlatforms. J. Electroanal. Chem. 166 (4), 249–257.
Sinha, A., Dhanjai Tan, B., Huang, Y., Zhao, H., Dang, X., Chen, J., Jain, R., 2018. MoS_2 nanostructures for electrochemical sensing of multidisciplinary targets: a review. Trac. Trends Anal. Chem. 102, 75–90.
Stanković, D.M., Mehmeti, E., Zavašnik, J., Kalcher, K., 2016. Determination of nitrite in tap water: a comparative study between cerium, titanium and selenium dioxide doped reduced graphene oxide modified glassy carbon electrodes. Sens. Actuators B Chem. 236, 311–317.
Sudarvizhi, A., Pandian, K., Oluwafemi, O.S., Gopinath, S.C.B., 2018. Amperometry detection of nitrite in food samples using tetrasulfonated copper phthalocyanine modified glassy carbon electrode. Sens. Actuators B Chem. 272, 151–159.
Sun, X., Wang, Z., 2018. Adsorption and diffusion of lithium on heteroatom-doped monolayer molybdenum disulfide. Appl. Surf. Sci. 455, 911–918.
Wang, J., Hui, N., 2017. A nanocomposite consisting of flower-like cobalt nanostructures, graphene oxide and polypyrrole for amperometric sensing of nitrite. Microchimica Acta 184 (7), 2411–2418.
Wang, P., Liu, Z.G., Chen, X., Meng, F.L., Liu, J.H., Huang, X.J., 2013. UV irradiation synthesis of an Au–graphene nanocomposite with enhanced electrochemical sensing properties. J. Mater. Chem. 1 (32), 9189.
Wang, J., Zhao, D., Zhang, Y., Li, J., Xu, C., 2014. A highly sensitive sensor for the detection of nitrite based on a nanoporous Fe_2O_3–CoO composite. Anal. Methods 6 (9), 3147–3151.
Wang, H., Chen, P., Wen, F., Zhu, Y., Zhang, Y., 2015. Flower-like Fe_2O_3@MoS_2 nanocomposite decorated glassy carbon electrode for the determination of nitrite. Sens. Actuators B Chem. 220, 749–754.
Wang, Y., Qu, Q., Li, G., Gao, T., Qian, F., Shao, J., Liu, W., Shi, Q., Zheng, H., 2016. 3D interconnected and multiwalled carbon@MoS_2@Carbon hollow nanocables as outstanding anodes for Na-ion batteries. Small 12 (43), 6033–6041.
Wang, Y., Ning, G., Bi, H., Wu, Y., Liu, G., Zhao, Y., 2018. A novel ratiometric electrochemical assay for ochratoxin a coupling Au nanoparticles decorated MoS_2 nanosheets with aptamer. Electrochim. Acta 285, 120–127.
Whitby, R.L.D., 2014. Chemical control of graphene architecture tailoring shape and properties. ACS Nano 8 (10), 9733–9754.
Xiong, F., Cai, Z., Qu, L., Zhang, P., Yuan, Z., Asare, O.K., Xu, W., Lin, C., Mai, L., 2015. Three-dimensional crumpled reduced graphene oxide/MoS_2 nanoflowers: a stable Anode for lithium-ion batteries. ACS Appl. Mater. Interfaces 7 (23), 12625–12630.
Xu, M., Liang, T., Shi, M., Chen, H., 2013. Graphene-like two-dimensional materials. Chem. Rev. 113 (5), 3766–3798.
Xu, W., Yi, H., Yuan, Y., Jing, P., Chai, Y., Yuan, R., Wilson, G.S., 2015. An electrochemical aptasensor for thrombin using synergetic catalysis of enzyme and porous Au@Pd core-shell nanostructures for signal amplification. Biosens. Bioelectron. 64, 423–428.
Xue, Y., Cai, W., Zheng, S., Yan, W., Hu, J., Sun, Z., Zhang, Y., Jin, W., 2017. W-doped MoS_2 nanosheets as a highly-efficient catalyst for hydrogen peroxide electroreduction in alkaline media. Catal. Sci. Tech. 7 (23), 5733–5740.
Yang, C., Lu, Q., Hu, S., 2006. A novel nitrite amperometric sensor and its application in food analysis. Electroanalysis 18 (22), 2188–2193.
Zhang, C., Wu, H.B., Guo, Z., Lou, X.W., 2012. Facile synthesis of carbon-coated MoS_2 nanorods with enhanced lithium storage properties. Electrochem. Commun. 20, 7–10.
Zhang, L., Wu, X., Yuan, Z., Lu, C., 2018a. π-Conjugated thiolate amplified spectrophotometry nitrite assay with improved sensitivity and accuracy. Chem. Commun. 54 (86), 12178–12181.
Zhang, X., Suo, H., Zhang, R., Niu, S., Zhao, X.q., Zheng, J., Guo, C., 2018b. Photocatalytic activity of 3D flower-like MoS_2 hemispheres. Mater. Res. Bull. 100, 249–253.
Zhang, Y., Zhou, Z., Wen, F., Tan, J., Peng, T., Luo, B., Wang, H., Yin, S., 2018c. A flower-like MoS_2-decorated $MgFe_2O_4$ nanocomposite: mimicking peroxidase and colorimetric detection of H_2O_2 and glucose. Sens. Actuators B Chem. 275, 155–162.
Zhao, Y., Zhou, J., Jia, Z., Huo, D., Liu, Q., Zhong, D., Hu, Y., Yang, M., Bian, M., Hou, C., 2019. In-situ growth of gold nanoparticles on a 3d-network consisting of a MoS_2/rGO nanocomposite for simultaneous voltammetric determination of ascorbic acid, dopamine and uric acid. Mikrochim. Acta 186 (2), 92.